Dakoulas, P. & Gazetas, G. (2008). *Géotechnique* **58**, No. 2, 95–111 [**doi:** 10.1680/geot.2008.58.2.95]

Insight into seismic earth and water pressures against caisson quay walls

P. DAKOULAS* and G. GAZETAS†

Motivated by the need to explain the large displacement and rotation that numerous caisson-type quay walls suffered in the port of Kobe during the devastating 1995 earthquake, a detailed numerical analysis is presented for the response of such a wall from Rokko Island. Utilising the Pastor–Zienkiewicz elastoplastic constitutive model, an effective stress dynamic analysis is performed using as input the accelerogram recorded 32 m below the ground surface in the nearby Port Island. The evolution during shaking of lateral displacements, plastic strains and pore water pressures sheds some light on the complex interplay of several simultaneously occurring phenomena: the development of oscillatory inertia forces on the wall, in phase or out of phase with the backfill soil and water pressures; the simple-shear seismic deformation of the soil and the ensuing initial development of positive excess pore water pressures in the backfill and the foundation soil; the extensional deformation developing in the 'active wedge' behind the wall, with the ensuing generation of negative excess pore water pressures; and the continuous dissipation and redistribution of water pressures. The conventional generalised Mononobe–Okabe theory is also reviewed, and extensive comparisons are made with the numerically computed effective and water pressures against the wall. Finally, a surprising role of the relative density of rubble behind the wall is highlighted.

KEYWORDS: case history; earth pressure; earthquakes; liquefaction; numerical modelling; retaining walls

Motivés par la nécessité d'expliquer les phénomènes de déplacement et de rotation importants auxquels un grand nombre de parois des quais du type à caisson du port de Kobe ont été soumis, lors du tremblement de terre catastrophique de 1995, nous présentons une analyse numérique détaillée de la réaction d'une paroi de ce type dans l'île de Rokko. En utilisant le modèle constitutif élastoplastique de Pastor-Zienkiewicz, nous effectuons une analyse dynamique des tensions efficaces, en utilisant, comme paramètre d'entrée, l'accélérogramme relevé à 32 mètres de profondeur dans Port Island, toute proche. L'évolution, au cours des secousses, des déplacements latéraux, allongements plastiques, et pressions interstitielles fournit des explications sur l'interaction complexe de plusieurs phénomènes se déroulant simultanément, par exemple le développement de forces d'inertie oscillatoires sur la paroi, en phase avec les pressions du sol de remblayage et de l'eau, ou déphasées par rapport à ces dernières ; la déformation sismique du sol à cisaillement simple, et le développement initial de pressions d'eau interstitielles positives excessives qui s'ensuivent dans le sol de remblayage et de fondation. ; le développement de déformations longitudinales dans les « coins actifs » derrière la paroi, avec la production des pressions d'eau interstitielles négatives excessives qui s'ensuit ; et la dissipation et redistribution continuelles des pressions d'eau. Nous examinons également la théorie généralisée traditionnelle de Mononobe-Okabe, et effectuons d'importantes comparaisons avec les pressions d'eau et efficaces calculées par ordinateur. Enfin, nous mettons en lumière un rôle surprenant du poids spécifique de la pierraille derrière le mur.

INTRODUCTION: OVERVIEW AND PROBLEM STATEMENT

In past earthquakes, concrete caisson quay walls subjected to strong shaking have repeatedly suffered substantial outward displacement and rotation, but have only rarely completely overturned. Nowhere was this more abundantly evident than in the port of Kobe during the 1995 earthquake (Hamada & Wakamatsu, 1996; Inagaki *et al.*, 1996, Kamon *et al.*, 1996), where wall displacements reached as much as 5 m with an outward tilting up to 5° (averages approximately 3 m and 2° respectively).

Liquefaction in the *backfill* was initially suspected or even proclaimed by some in the geotechnical community as the main villain behind such large deformations. However, observations in the field failed to reveal any signs of liquefaction on the backfill surface near the wall, within a distance of about $2H$ (i.e. twice the height of the wall) (Towhata *et al.*, 1996; Iai *et al.*, 1998).

A more recent case history of a similar example (but smaller in scale) where no liquefaction occurred next to a substantially displaced quay wall was observed in the Lefkada M_s 6·4 earthquake in Greece (14 August 2003). Having a concrete cross-section of 5 m × 5 m for a depth of water of only 3·5 m, this wall was supported on sandy gravel and clayey sand. It displaced laterally about 25 cm (maximum) owing to an acceleration history involving at least seven cycles of motion with peaks in the range 0·25–0·45g. No sign of liquefaction was noticed in the immediate backfill, although such evidence did appeared 10–20 m away from the wall (Gazetas *et al.*, 2005).

For Kobe, subsequent comprehensive theoretical and experimental research has shed light on the complicated behaviour of the quay wall–soil system. Among the most significant findings of the research so far are the following.

(*a*) The displacement of the wall could be attributed to two factors:
   (i) the significant lateral pressures from the backfill and the large inertia of the wall itself, as the driving forces
   (ii) the strongly inelastic deformation of the foundation soil, allowing the caisson to move and tilt, as the

Manuscript received 23 March 2006; revised manuscript accepted 17 October 2007.
Discussion on this paper closes on 1 September 2008, for further details see p. ii.
* Department of Civil Engineering, University of Thessaly, Volos, Greece.
† School of Civil Engineering, National Technical University, Athens, Greece.

supporting soil beneath the caisson was 'pushed out' (Iai *et al.*, 1998).

(*b*) Liquefaction occurred *only* in the free field away from the wall, not in the backfill next to the wall. In the foundation soil, on the other hand, very substantial excess pore water pressures developed, undermining its stiffness and strength. This facilitated the lateral translation and rotation of the wall (Ghalandarzadeh *et al.*, 1998), even though 'complete' liquefaction did not develop (Towhata *et al.*, 1996).

(*c*) Of the two driving forces, the wall inertia played the most detrimental role, whereas the earth and water pressures from the backfill were of lesser importance (Ghalandarzadeh *et al.*, 1998; Sato *et al.*, 1998).

(*d*) The outward movement of the caisson stopped at the end of shaking—an analytical and experimental finding consistent with the previous conclusions. This provides further evidence that the whole phenomenon is driven mainly by wall inertia and not by liquefaction flow (Ghalandarzadeh *et al.*, 1998; Sato *et al.*, 1998). In fact, use of the term 'lateral spreading' for the deformations observed behind the Kobe quay walls may not be suitable for describing the whole phenomenon.

All these findings are broadly consistent with the results of earlier studies. For example, Zeng (1993), using centrifugal modelling, had found out that the pore water pressures did not increase behind the wall, although liquefaction was triggered in the 'free' field, and that the wall lateral displacement terminated upon the end of ground shaking. However, some other studies have pointed in, apparently, the opposite direction. For example, Sugano *et al.* (1995) claimed that extensive liquefaction was observed behind a model wall that rested on dense sand. But perhaps it was the small size of the lateral outward displacement of the wall (due to the substantial foundation stiffness) that did not allow for any significant lateral extension and consequent reduction of the positive excess pore water pressures, as such positive pressures were being generated by the vertically propagating shear waves. Such a reduction would have prevented liquefaction, as was the case in Kobe, and will be explained later in the paper.

Another topic of interest refers to the magnitude of the developed earth and water pressures, and their relationship with the Mononobe–Okabe and Westergaard theories (Okabe, 1926; Mononobe & Matsuo, 1929; Westergaard, 1933). One thing is clear from most experimental tests (both shaking table and centrifuge): *strain localisation*, defining a Coulomb-type active failure surface, almost always occurs, and limits the magnitude of earth pressures to Mononobe–Okabe levels. The phasing, however, of the resultant earth pressure in comparison with the wall inertia force remains a topic of rather wide disagreement. A brief reference is made here, first, to the work of Al-Homoud & Whitman (1999), who analysed numerous finite element and centrifuge results for walls retaining *dry* soil and concluded that: (a) at the time of maximum outward tilt, most of the dynamic overturning moment comes from horizontal inertia of the wall, whereas the earth thrust is unimportant; (b) the Seed–Whitman (1970) or Mononobe–Okabe methods overpredict the dynamic earth thrust.

Other researchers, however, found satisfactory agreement between Mononobe–Okabe and measurements for dry sandy soil (e.g. Fujiwara *et al.*, 1999). For the quay walls that are of interest here, in particular, the situation becomes far more complicated because of the following four phenomena that occur simultaneously:

(*a*) The development of oscillatory wall inertia loading, which tends to produce outward displacement and rotation of the wall due to the compliance of the supporting soil.

(*b*) The simple-shear deformation of the backfill from the (incident and reflected) vertically propagating shear waves, which tends to generate positive excess pore water pressures $+\Delta u$ in the (usually loose) underwater-placed soils. In the free field, the accumulated build-up of such pressures may lead to liquefaction.

(*c*) Extensional normal deformation of the backfill soil adjacent to the wall, as the wall moves outwards. This tends to generate negative excess pore water pressures $-\Delta u$, which may or may not overshadow the positive seismic pore water pressures, depending on the amount and speed of the wall movement, as well as on the density of soil. (Dense dilatant soil in extension may develop exceedingly large *negative* water pressures.)

(*d*) The tendency to continuous dissipation and redistribution of pore water pressures (flow in two dimensions), eventually resulting in a detrimental 'contamination' of the regions of negative excess pore water pressure (which therefore become neutralised or even change their sign to positive) towards the end of shaking.

Evidently, the whole problem is very complex, and with the present state of knowledge there is no clear understanding of how sensitive each of the above simultaneous phenomena is to variations in soil characteristics (imperfectly known in reality) such as the relative density and the coefficient of permeability of the various constituent soils.

To fill this important gap in understanding, the main goal of this paper is to assess the interplay among developing excess pore water pressures, earth thrusts, foundation deformations, and wall movement, and to highlight a potential significance of the *soil density behind the wall*. To this end, the paper utilises the rigorous finite difference formulation of FLAC (Itasca, 2000), together with a comprehensive elastoplastic effective-stress constitutive soil model developed by Pastor *et al.* (1990) and implemented by Dakoulas (2003). A second goal is to compare the developing earth and water pressures with the conventionally applied Mononobe–Okabe and Westergaard pressures. All this is done within the framework of a case history from Kobe, involving the response of a quay wall in Rokko Island, whose large outward displacement and tilting have been documented and analysed by Iai and his co-workers in a number of publications (Inagaki *et al.*, 1996; Iai, 1998; Iai *et al.*, 1998).

BENCHMARK CASE HISTORY: ROKKO ISLAND QUAY WALL

The numerous case histories from the Kobe port offer a valuable source of field data against which to check new methods of analysis, and with which to uncover phenomena that are not well understood at present. Fig. 1 shows a plan of the city of Kobe, together with the approximate location of the strike-slip fault of the 1995 earthquake, and some key points of interest in this paper.

Most quay walls in Kobe were of the caisson type. They had been designed pseudo-statically, with seismic coefficients ranging from 0·10 to 0·25, depending on site conditions, year of construction, and the importance of the facility. They had been placed on top of gravelly fill consisting of decomposed granite (called locally 'Masado'), which had completely replaced the soft clay layer beneath the caisson for improving the bearing capacity and reducing settlements. The most severe damage occurred in those caisson walls of Port and Rokko Islands that: (a) were nearly parallel to the coastline (and thus parallel to the causative

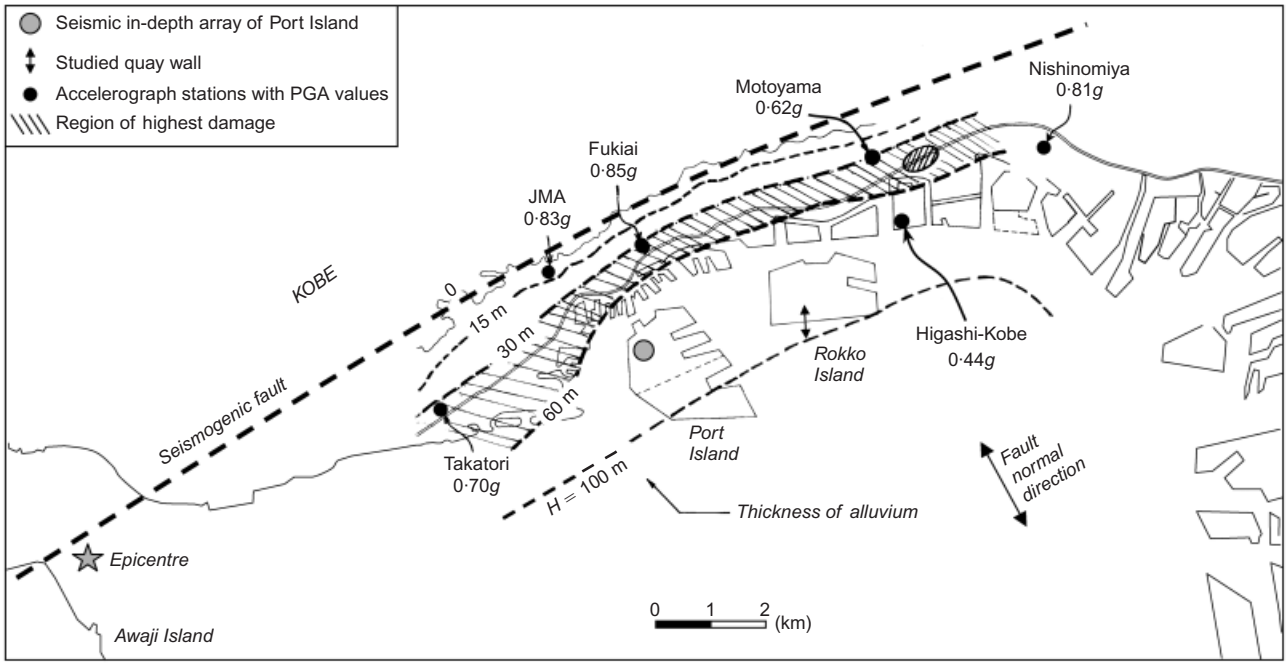

Fig. 1. Map of Kobe showing seismologically inferred 1995 earthquake fault, location of studied quay wall (double arrow), and accelerograph stations showing the recorded peak ground accelerations (PGA) and shaded region of highest structural damage. The location of the $M_{JMA} = 7{\cdot}2$ fault is drawn approximately, since it did not emerge on the ground surface in Kobe; it only did so in Awaji Island (lower left corner). The city of Kobe covers approximately all the area between the fault and the sea (Osaka Bay)

fault), and thereby experienced the stronger fault-normal accelerations (Somerville, 1998); and/or (b) had been designed with a small seismic coefficient, of 0·10 to 0·15. By contrast, the caisson wall of the main wharf at Maya Futo, designed conservatively with a large seismic coefficient of 0·25 and running almost perpendicular to the fault (and thereby having been subjected to some less severe accelerations parallel to the fault), did not experience any visible damage or substantial deformation, remaining operational after the earthquake. It is worth mentioning that, despite the large deformations, the caissons did not overturn. Their overall performance can be judged as better than that of the alternative quay wall system, the *anchored sheet-pile wall*, which in earlier earthquakes that were much less devastating than the Kobe 1995 earthquakes were frequently experiencing collapsing failures (e.g. Kitajima & Uwabe, 1978, Gazetas *et al.*, 1990).

The case history corresponds to the typical quay wall section of Rokko Island, in which both the foundation and backfill soils are liquefiable. The location of the wall is shown in Fig. 1. A cross-section of the quay wall with its deformation recorded after the earthquake is reproduced from Iai *et al.* (1998) in Fig. 2. The finite-difference discretisation and the material zones used in our analyses are shown in Fig. 3. During the earthquake the wall top displaced approximately 4 m seaward (exceeding 5 m in a

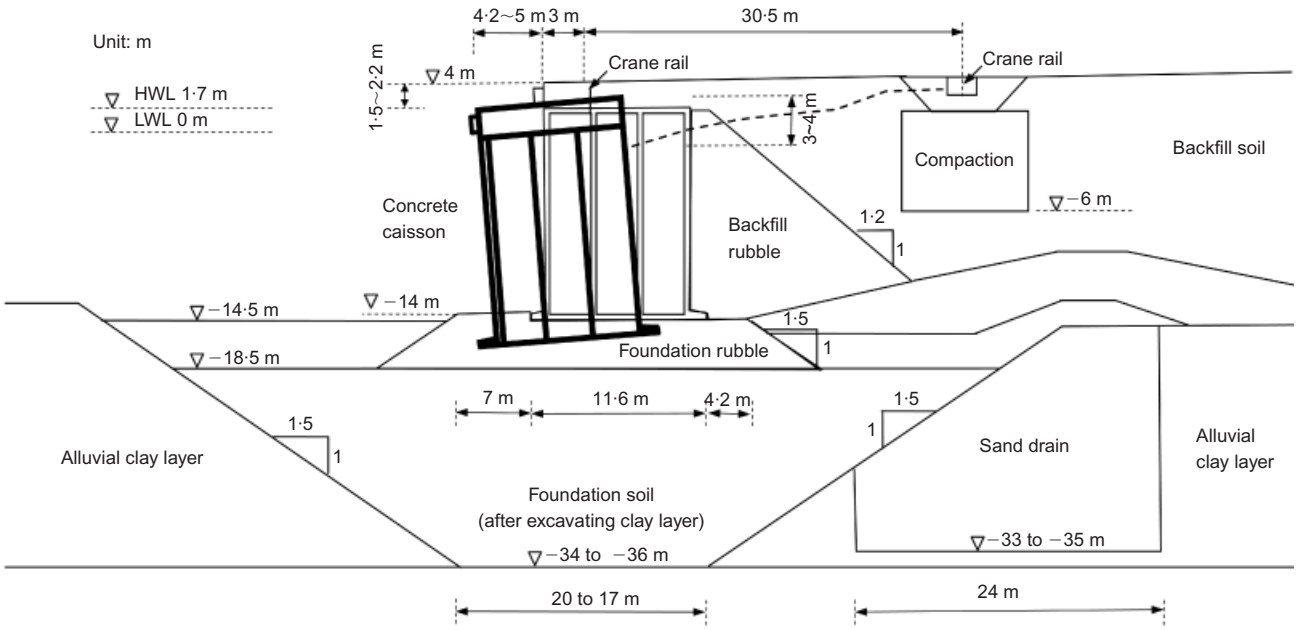

Fig. 2. Cross-section of caisson quay wall RC-5 in Rokko Island and its residual deformation observed after Kobe 1995 earthquake (from Iai *et al.*, 1998)

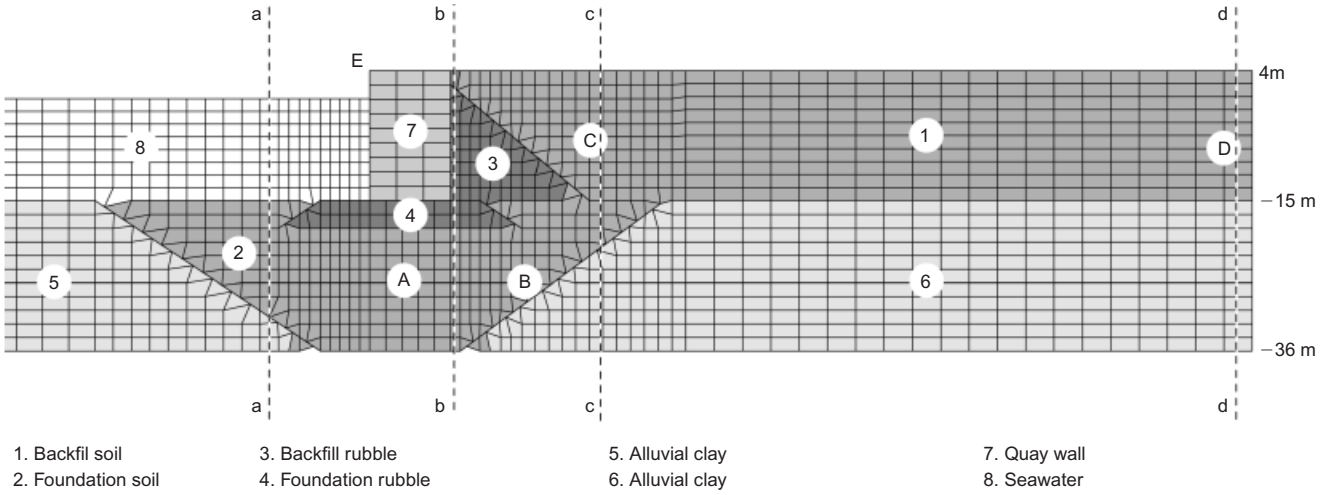

Fig. 3. Geometry (in natural scale), finite difference discretisation, and material zones of Rokko Island quay wall system. Points A, B, C and D and lines aa, bb, cc and dd are for showing details of pore water pressures and displacements

few locations). It settled about 1–2 m and tilted about 4° outwards. Despite these significant movements, the site investigation showed no collapse of the wall along its entire length. Also, no evidence was observed of liquefaction either within a zone extending about 30 m behind the wall or near the toe of the wall in the sea. However, evidence of liquefaction was abundant farther away in the free field (Towhata *et al.*, 1996, Iai *et al.*, 1998, Inagaki *et al.*, 1996). Investigation by divers cited by Inagaki *et al.* (1996) revealed substantial heaving of the foundation rubble at a distance of 2–5 m in front of the toe of the caisson—indicative of 'squeezing out' of the soil underneath the edge (toe) of the tilting caisson.

Detailed information about standard penetration test (SPT) N values at various depths, grain-size distributions, plasticity indexes, S-wave velocities, and cyclic triaxial test data have been presented by Inagaki *et al.* (1996). The density, initial shear modulus, and friction angle in Table 1 were adopted from Iai *et al.* (1998). Of importance in our analysis is the contractiveness of the decomposed granite material (Torii & Tatsuoka, 1982), as will be discussed later.

The above case history is analysed in this paper using a state-of-the-art effective stress dynamic elastoplastic analysis. The conventional method of determining dynamic earth pressures pseudostatically is also being used to provide a basis of comparison with the numerical results.

CONVENTIONAL EARTH AND WATER PRESSURES

At present, seismic active earth pressures are still being determined conventionally with the so-called Mononobe–Okabe method, developed in the 1920s as an extension of Coulomb's limiting equilibrium method (Okabe, 1926; Mononobe & Matsuo, 1929).

Table 1. Material properties for the Rokko Island quay wall foundation and backfill soils (Iai *et al.*, 1998)

Material	Density: Mg/m^3	G_{max}: MPa	σ'_0: kPa	ϕ: degrees
Foundation (Zone 2)	1·8	58	106	37
Backfill (Zone 1)	1·8	79	63	37
Alluvial clay (Zones 5, 6)	1·7	75	143	30
Rubble (Zones 3, 4)	2	80	98	40
Caisson wall	2·1			

Friction angle at caisson bottom = 30°. Friction angle at caisson back = 15°.

The method involves a pseudo-static analysis where the effect of an earthquake excitation (characterised by a horizontal and a vertical component of 'effective' acceleration, $\alpha_h g$ and $\alpha_v g$ respectively**)**, is modelled by imposing an additional set of forces on the dynamic equilibrium of a trial wedge: a lateral force $\alpha_h W$ and a vertical force $a_v W$, in which W is the weight of the wedge. [The 'effective' seismic coefficients are denoted herein as α_h and α_v, instead of the prevailing symbols k_h and k_v which would have been doubly unfortunate in this case: (a) for a symbol of a spatially averaged acceleration there is no rationale for changing from α to k ; (ii) since k is used in this paper for the coefficient of permeability **(**and also, in general, for the modulus of Winkler springs**)**, adopting it for acceleration might only create some unnecessary confusion.]

The quay wall problem studied in this paper does not fall strictly within the domain of the Mononobe–Okabe (M-O) assumptions, for a variety of reasons that will become evident in the sequel, not least of which is the occurrence of liquefaction in the backfill. Nevertheless, we utilise the M-O method in order to obtain a yardstick for evaluating the magnitude of the time-dependent earth pressures. To this end we select the basic value for the seismic coefficient as a function of the peak ground acceleration, adopting the Japanese procedure proposed by Noda *et al.* (1975). First, however, we have to disregard the sole 0·54g spike of the record in Fig. 4 (at −32 m) as being of an extremely short duration to be 'felt' by any structure. Instead, we consider as the essential peak acceleration $A \approx 0{\cdot}40g$

Then the empirical relationship of Noda *et al.* (1975) for the seismic coefficient as a function of A,

$$\alpha_h = \frac{1}{3}\left(\frac{A}{g}\right)^{\frac{1}{3}} \tag{1}$$

yields $\alpha_h = 0{\cdot}25$, a value that, incidentally, is only slightly larger than the design seismic coefficient ($\approx 0{\cdot}20$).

Whereas in most of our subsequent numerical studies the recorded vertical component of acceleration (at −32 m) has also been used to define the excitation as rigorously as possible, numerous parametric studies have unequivocally shown that vertical acceleration has practically no appreciable effect on the response of the quay wall system—especially this particular very high-frequency vertical acceleration. This is in accord with several other studies on the

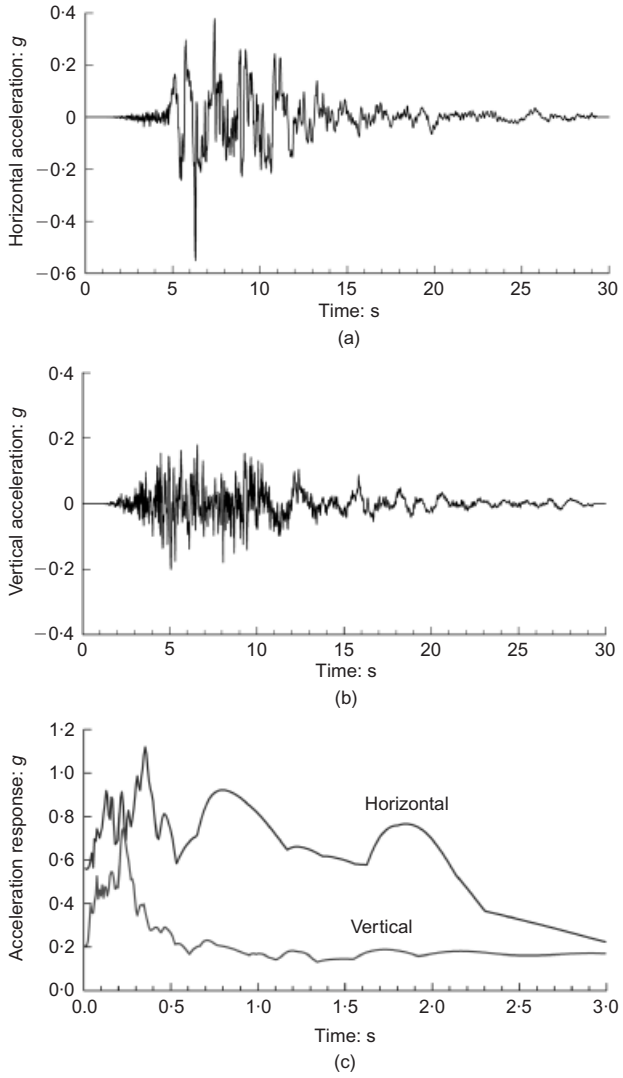

Fig. 4. Input excitation—two components of ground motion recorded in nearby Port Island seismograph array at depth of 32 m, during 1995 Kobe earthquake: (a) horizontal NS component; (b) vertical component; (c) corresponding acceleration response spectra (adapted from Iwasaki & Tai, 1996)

subject (e.g. Seed & Whitman, 1970; Gazetas *et al.*, 2004), as well as with the recommendations of Japanese (JSCE, 2000; OCDI, 2002) and international (PIANC, 2001) codes. We therefore ignore (in this application of the conventional method) the vertical component of acceleration. However, the subsequent numerical analysis takes both the horizontal and vertical components of excitation into account.

The M-O expression for the total (static plus dynamic) active earth-pressure force is

$$P_{AE} = \tfrac{1}{2}\gamma H^2 K_{AE} \tag{2a}$$

where

$$K_{AE} = \frac{\cos^2(\phi - \psi)}{\cos\psi\cos(\psi + \delta)\left\{1 + \left[\sin(\phi + \delta)\sin(\phi - \psi)/\cos(\delta + \psi)\right]^{\frac{1}{2}}\right\}^2} \tag{2b}$$

in which ϕ is the angle of shearing resistance of the retained soil, and δ is the angle of friction along the vertical wall−soil interface. The angle ψ is a function of the apparent seismic coefficient α'_h:

$$\psi = \arctan(\alpha'_h) \tag{3}$$

The value of α'_h reflects not only the level of the basic seismic coefficient α_h (0·25 in this case), but also the effect of submergence in water (Matsuzawa *et al.*, 1985; Ebeling & Morison, 1992).

For dry retained soil $\alpha'_h = \alpha_h$, and of course the unit weight γ in equation (2a) is simply the dry unit weight γ_{dry}. For a fully submerged backfill

$$\alpha'_h = \alpha_h \frac{\gamma_{sat}}{\gamma_b} \tag{4}$$

and the submerged unit weight $\gamma_b = \gamma_{sat} - \gamma_w$ must replace γ in equation (2a) to compute P_{AE}. The resultant of the static water pressures must be added to this value. The underlying assumptions for the above treatment of a submerged backfill are that: (a) pore water pressures do not change as a result of horizontal motion; and (b) that backfill permeability is low enough for the water to move as a unit with the mineral skeleton. According to the PIANC (2001), manual the threshold permeability for the latter condition is of the order of $k \approx 10^{-4}$ m/s.

For a partially submerged backfill, as in this case (the water table in Rokko island is at sea level, i.e. 4 m below the top of the retained soil), weighting thrusts based on the volume of soil in the failure wedge below and above the water surface result in the following expressions for the *apparent seismic coefficient* of an equivalent 'homogeneous' soil (PIANC, 2001),

$$\alpha'_h = \alpha_h \frac{\gamma_{sat} H_w^2 + \gamma H_{sur}^2 + 2\gamma H_w H_{sur}}{\gamma_b H_w^2 + \gamma H_{sur}^2 + 2\gamma H_w H_{sur}} \tag{5}$$

and the effective unit weight of soil,

$$\gamma' = \gamma_b \left(\frac{H_w}{H}\right)^2 + \gamma\left[1 - \left(\frac{H_w}{H}\right)^2\right] \tag{6}$$

in which $H = H_w + H_{sur}$ is the total height of the wall; H_w is the height below the water surface, where the buoyant unit weight γ_b controls; and H_{sur} is the height above the water surface, where the soil is not in buoyancy and has a unit weight γ. Equations (5) and (6) are used in equations (2) and (3) to determine the effective static-plus-dynamic earth thrust. In this particular case $H_w = 14$ m, $H_{sur} = 4$m, $\gamma = 18$ kN/m^3, and $\gamma_b = 10$ kN/m^3. Therefore

$$\gamma' \approx 13{\cdot}2 \text{ kN/m}^3, \quad \alpha'_h \approx 0{\cdot}37 \tag{7}$$

$$K_{AE} \approx 0{\cdot}52 \text{ and } P_{AE} \approx 1112 \text{ kN/m} \tag{8}$$

For the static active earth pressure,

$$K_A \approx 0{\cdot}25 \text{ and } P_A \approx 535 \text{ kN/m} \tag{9}$$

Hence the *dynamic* effective earth pressure and its horizontal component, assuming $\delta = \phi/2 \approx 18{\cdot}7°$, are

$$\begin{aligned} \Delta P_{AE} &\approx 577 \text{ kN/m} \\ (\Delta P_{AE})_x &= (P_{AE} - P_A)\cos\delta \approx 547 \text{ kN/m} \end{aligned} \tag{10}$$

During seismic shaking, excess pore water pressures Δu are generated; they are expressed through the dimensionless parameter

$$r_u = \frac{\Delta u}{\sigma'_{v0}} \tag{11}$$

in which σ'_{v0} is the initial vertical effective stress. The M-O method cannot rigorously account for Δu, especially in the general case in which Δu and r_u are different functions of depth; $\Delta u = \Delta u(z)$, $r_u = r_u(z)$.

Only when the backfill is fully submerged is Δu is

proportional to σ'_{v0}, and r_u is therefore constant independent of depth, can we adopt the following approximations of Ebeling & Morison (1992).

(*a*) Effective unit weight of soil:

$$\gamma_e = \gamma_b(1 - r_u) \tag{12}$$

(*b*) Apparent seismic coefficient:

$$\alpha'_h = \alpha_h \frac{\gamma_{sat}}{\gamma_e} \tag{13}$$

(*c*) Effective unit weight of water:

$$\gamma_{we} = \gamma_w + \gamma_b r_u \tag{14}$$

Equations (12) and (13) are used in equations (2) and (3) to compute the effective static-plus-dynamic earth thrust $P_{AE,}$ and equation (14) is used to compute the quasi-static water pressures (Ebeling & Morrison, 1992). As an example (to be utilised later), for a hypothetical negative excess pore water pressure, with $r_u = -0{\cdot}50$, we obtain

$$\gamma_e \approx 20 \text{ kN/m}^3, \ \gamma_{we} \approx 3{\cdot}4 \text{ kN/m}^3, \ \alpha'_h \approx \alpha_h = 0{\cdot}25 \tag{15}$$

$$K_{AE} \approx 0{\cdot}32 \text{ and } P_{AE} \approx 1038 \text{ kN/m} \tag{16}$$

The latter value is essentially the same as P_{AE} for $r_u = 0$ (equation (8)), but the water pressures are about one-third of their hydrostatic 'predecessors'.

However, as a positive r_u approaches unity (initiation of liquefaction), the effective unit weight tends to vanish (equation (12)), while the unit weight of water approaches the total unit weight of saturated soil:

$$\gamma_{we} = \gamma_w + \gamma_b = \gamma_{sat} \tag{17}$$

In this case it would be necessary to superimpose the hydrodynamic pressures of this 'fluid', using the Westergaard gaard(1933)relationship

$$P_h = \tfrac{7}{12}\alpha_w \gamma_{sat} H_w^2 \tag{18}$$

where α_w is the *wall* acceleration coefficient (conventionally taken to be equal to the seismic coefficient α_h).

The M-O solution does not provide any direct information on the point of action of the resulting earth force—just as the Coulomb analysis does not by itself give the distribution of static pressures. Evidently, dynamic pressure distributions along the back of the retaining wall depend upon both the magnitude of wall movement and the mode in which these movements occur.

Experimental results obtained in the last 50 years have indicated that for gravity retaining walls (such as the quay walls studied here but with dry soil) the vertical position of the resultant static-plus-dynamic force P_{AE} ranges from $0{\cdot}40H$ to $0{\cdot}50H$ from the base of the wall, where H is the height of the retained soil. This implies that, since the static component P_A is conventionally presumed to act at $\frac{1}{3}H$ (the result of a presumed Rankine-type triangular distribution), the dynamic component would act at about $0{\cdot}50H$ to $0{\cdot}65H$ (e.g. Seed & Whitman, 1970). The intuitive explanation given for this higher position of the dynamic force as found in experiments is that the soil mass of the horizontally moving sliding wedge is largest at the top of the wall and smallest at its base, and so the inertia force on the wedge is concentrated near the top.

This is hardly a complete argument, and in any case it is not entirely convincing. Moreover, most of the small-scale shaking-table experiments that seemed to suggest the higher location of the dynamic active force involved primarily horizontal sliding of the wall, with little or no rotation. Recent theoretical analyses by Veletsos & Younan (1997) have shown that, with increasing rotational flexibility at the base of the wall, the location of the dynamic earth thrust moves from about $\frac{2}{3}H$ for a wall fixed rotationally at its base down to $\frac{1}{3}H$—the latter value implying a triangular (Rankine type) distribution of earth pressures against the wall.

In the case of the Kobe quay wall studies that are reported here we note that

(*a*) rotation is an important component of the wall movement
(*b*) the retained soil is only partially submerged (14 out of 18 m under the sea)
(*c*) 'excess' pore water pressures leading up to liquefaction may have developed.

It is thus not obvious how the conventional M−O based method would apply. Nevertheless, this method is used in this paper *only* to provide a *reference solution* against which to appreciate and interpret the rigorous results obtained numerically. To this end, we shall assume that the 'conventional' earth and water pressures are computed from the pertinent equations (1)–(6) and (11)–(16), with the resultant dynamic earth force acting at the mid-height of the wall, as if earth pressures were uniformly distributed with depth. (The alternative of choosing the one-third height from the base as the location of the resultant, which would be consistent with a linear pressure distribution, would have also been a logically crude approximation.)

EFFECTIVE STRESS NUMERICAL INELASTIC ANALYSIS

The soil constitutive model

A 'rigorous' effective stress method of analysis is applied here to analyse the response of the above quay wall. A finite-difference commercial code (FLAC) is utilised in conjunction with a comprehensive elastoplastic model for cohesionless soils. The latter was developed by Pastor *et al.* (1990), and was slightly modified and attached to FLAC (Itasca, 2000). The model was developed within the framework of generalised plasticity; it avoids some complexities associated with classical plasticity, while allowing greater computational efficiency. It is based on the critical-state theory, which postulates that all residual states lie on a unique line in p'–q–e space, regardless of the stress path followed. Consistently with experimental evidence for cohesionless soils, the model uses a non-associative flow rule for modelling the behaviour within the hardening region. The model does not require the explicit definition of the yield and potential functions, but only of the direction vectors normal to each surface. The direction of the plastic strain increment vector depends on dilatancy, which is approximated by a linear function of the stress ratio $\eta = q/p'$. In contrast to classical plasticity, the model does not require the application of the consistency condition to define the hardening modulus. This considerably simplifies the computational aspects and improves computational efficiency. Detailed descriptions of the basic model are given in the original publications by Pastor *et al.* (1985, 1990), Pastor & Zienkiewicz (1986), and Zienkiewicz *et al.* (1985, 1991, 1999).

For loose *contractive* sand the model predicts the densification and strain-hardening in drained shear, and the development of excess pore pressure and liquefaction in undrained shear. For very dense *dilative* sands in drained shear, the model accounts for strain-softening and residual conditions at the critical state. Comparisons between predictions of the original model and experimental data on undrained monotonic loading of contractive and dilative sands,

on cyclic loading leading to liquefaction of very loose sands, and on cyclic mobility of dense sands showed very good agreement (Pastor *et al.*, 1990).

The plastic modulus for unloading, H_U, has been modified from the original form (Pastor *et al.*, 1990) in order to incorporate the stress dependence, and is expressed as

$$H_U^* = \begin{cases} H_{uo}\, p' \left(\dfrac{M_g}{\eta_u}\right) & \text{if } \left|\dfrac{M_g}{\eta_u}\right| > 1 \\ H_{uo}\, p' & \text{if } \left|\dfrac{M_g}{\eta_u}\right| \leqslant 1 \end{cases} \tag{19}$$

where H_U^* is the modified modulus; H_{uo}, γ_u are model parameters; p' is the effective mean stress; and η_u is the stress ratio from which unloading takes place.

A systematic series of comparisons between predictions of the modified model and experimental data for different sands from both monotonic and cyclic tests in compression–extension and simple shear showed very good agreement (Dakoulas, 2003). Overall, the model seems capable of describing soil behaviour realistically under monotonic and cyclic loading for a wide range of relative densities. It is being used to simulate approximately the soil response under seismic conditions.

Numerical model and analysis

The geometry discretisation and the material zones of the numerical model for all analyses considered are illustrated in Fig. 3. The cohesionless material in the foundation zone, the backfill zone and the (foundation and backfill) rubble zones is modelled utilising the elastoplastic constitutive model by Pastor *et al.* (1990). The clay zones are modelled approximately using the Mohr–Coulomb model with properly adjusted material parameters based on independent equivalent linear analysis. The seawater mass is modelled as a saturated, elastic sponge, having the density and the bulk modulus of the water, and an artificial, very small value of the shear modulus that is necessary to avoid numerical problems. Finally, the wall is modelled as an elastic body, having an interface that allows slippage and separation at the base and the back of the caisson.

In the course of the present investigation the following types of analysis were performed: (a) one considering a variable relative density within the foundation and backfill zones based on the SPT blow count variation (Cubrinovski & Ishihara, 1999); and (b) a second considering a uniform distribution of an equivalent relative density of 35%. No significant differences were noted in the results. Thus only those from the uniform distribution are presented here. Although the value of $D_r = 35\%$ is an approximation, given the variability in density of the decomposed granite soil, it is adopted here in order to simplify the interpretation, and thereby allow an easier comparison between the response of natural and improved soil. In fact, comparisons between computed and actual response discussed below indicate that, in a significant part of the quay wall in Rokko Island, the equivalent relative density of the foundation or backfill soil might have been even lower than 35%. The foundation rubble and the backfill rubble (on the back of the wall) were considered with a relative density D_r parametrically varied to take values of 40% and 60%. The model parameters for relative densities 35%, 40% and 60% are given in Table 2.

For the seismic excitation of our model we also adopted the choice of many researchers, including Iai *et al.* (1998): the horizontal (NS) and vertical components of the accelerogram recorded at a depth of 32 m in the Port Island array (Iwasaki & Tai, 1996), whose peak acceleration values reached 0·54*g* and 0·20*g* respectively. Fig. 4 plots the two

Table 2. Model parameters for three relative densities

Material parameter*	$D_r = 35\%$	$D_r = 40\%$	$D_r = 60\%$
K_0	35 200	36 200	40 300
M_{gc}	1·44	1·47	1·57
M_{fc}	0·35	0·40	0·67
α	0·47	0·48	0·50
H_0	350	365	500
β_0	6	6	6
β_1	0·6	0·6	0·6
γ	4	4	4
H_{u0}	2000	2000	2000
γ_u	2	2	2

* The definitions of the model parameters and the associated constitutive equations may be found in the original paper by Pastor *et al.* (1990).

accelerogram components and their acceleration response spectra. The choice is reasonable in view of the nearly equal distance of the two sites (in Port and Rokko islands) from the seismogenic fault, the similarity in stiffness of the underlying 'base' soil where the recorded motion is applied, and the broad similarity in overall thickness and stiffness of the respective soil deposits. Note in passing that, owing to substantial forward-rupture directivity effects in the Kobe earthquake, ground motions normal to the fault were significantly stronger (especially in long-period components) than fault-parallel motions: hence the orientation of a particular wall is important in choosing a most probable excitation. The particular wall examined here runs almost parallel to the EW direction: hence our choice of the NS recorded component as its lateral excitation is justified. Nevertheless, the selection of excitation unavoidably introduces a small uncertainty in our results.

RESULTS OF NUMERICAL STUDY USING PUBLISHED SOIL PARAMETERS

The results for the response of the system are presented through the following graphs:

(*a*) cross-sections with contours of horizontal displacement, excess pore water pressure, and plastic shear strain, at certain times during shaking. Plastic shear strain is computed from

$$\begin{aligned} \varepsilon_s^p &= \frac{2}{\sqrt{3}}\sqrt{J_2^{\varepsilon p}} \\ &= \frac{1}{3}\left\{2\left[\left(\varepsilon_{22}^p - \varepsilon_{33}^p\right)^2 + \left(\varepsilon_{33}^p - \varepsilon_{11}^p\right)^2 + \left(\varepsilon_{11}^p - \varepsilon_{22}^p\right)^2\right] \right. \\ &\quad \left. + 3\left(\gamma_{12}^p\right)^2\right\}^{\frac{1}{2}} \end{aligned} \tag{20}$$

where ε_{11}^p, ε_{22}^p, ε_{33}^p and γ_{12}^p are the plastic strain components, and $J_2^{\varepsilon p}$ is the second invariant of the deviatoric plastic strains

(*b*) time histories of the horizontal and vertical displacement of the caisson top

(*c*) time histories of the excess pore water pressures at selected points in the backfill and the foundation

(*d*) distributions with depth of the residual horizontal displacements along several vertical lines behind and in front of the wall

(*e*) distribution with depth of the horizontal effective earth and water pressures acting on the back of the wall.

We then present a brief investigation of the influence of the relative density of the rubble in the backfill soil and of the coefficient of permeability.

Displacements, strains, and water pressures reveal a major detrimental role of the foundation soil

Figure 5 portrays the contours of horizontal displacement at four different moments in the history of shaking: $t = 7{\cdot}5$, 9·0, 30 and 38 s. The end of strong shaking is at $t = 30$ s. (The seawater mesh has been removed from the plots for clarity.) Fig. 5 should be studied together with Fig. 6, which plots the time history of the horizontal and vertical displacements at the upper left (sea-side) corner of the wall, and Fig. 7, which shows the distribution of horizontal displacements with depth at four vertical lines (aa, bb, cc, dd).

At the end of earthquake shaking, the sea-side corner of the wall is computed to have moved by about 4·5 m horizontally and to have settled 1·9 m. The deformed mesh in Fig. 5(d) shows that the retained soil behind the wall settled significantly (with a maximum settlement of about 2·2 m), following the seaward movement of the wall. These displacements are in excellent accord with the field observations, with the exception of the implied tilt: 1°, compared with the measured 5° and the 4° computed by Iai and his co-workers.

Moreover, the foundation rubble was substantially deformed underneath the seaward edge of the foundation, as can be discerned in Fig. 5; in the profile 'aa' of residual displacements shown in Fig. 7; and in the contours of excess

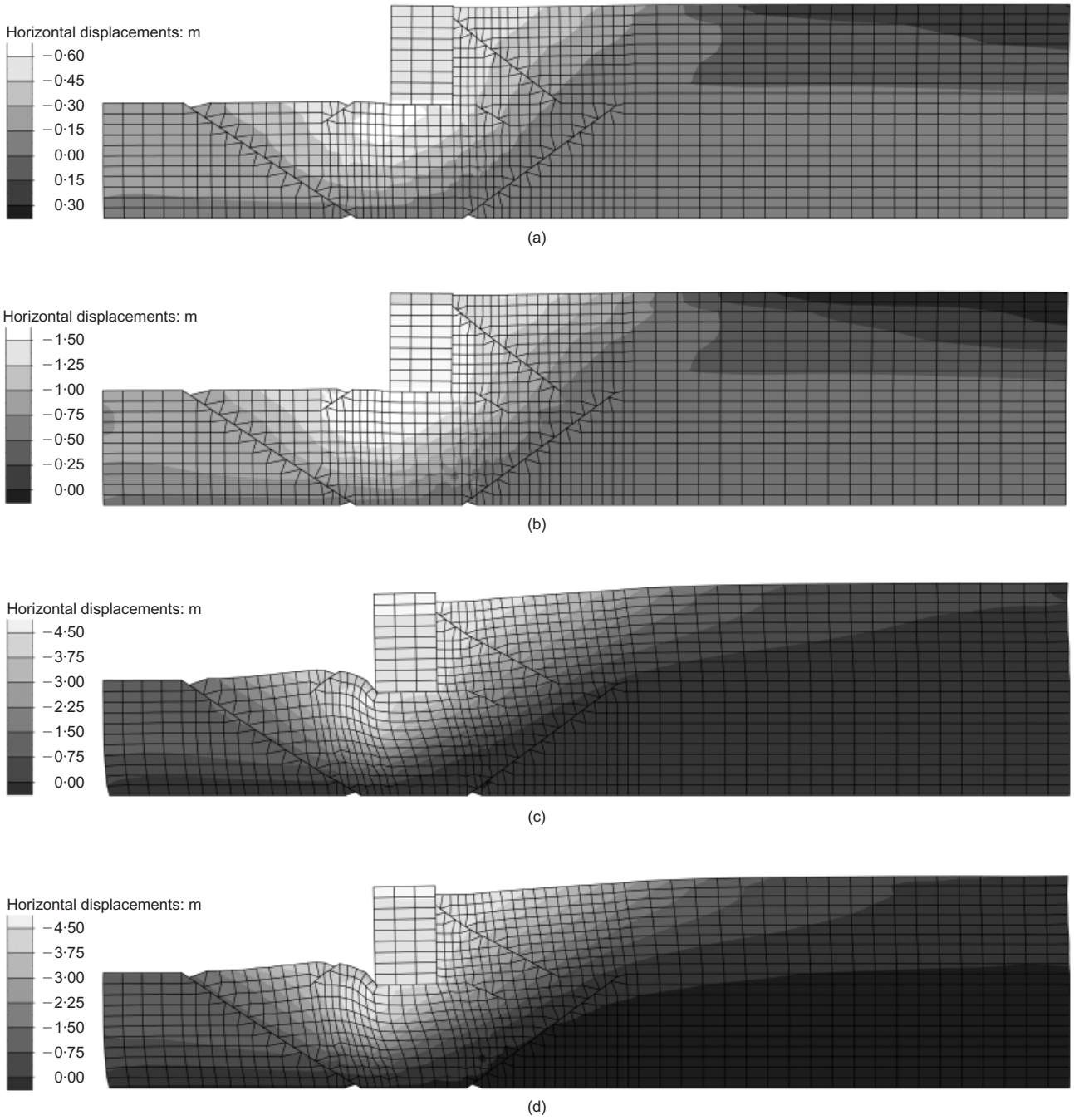

Fig. 5. Deformed geometry and contours of horizontal displacements of the quay wall at various times *t*: (a) 7·5 s; (b) 9 s; (c) 30 s; (d) 38 s (backfill and foundation rubble: $k = 4 \times 10^{-4}$ m/s; $D_r = 40\%$)

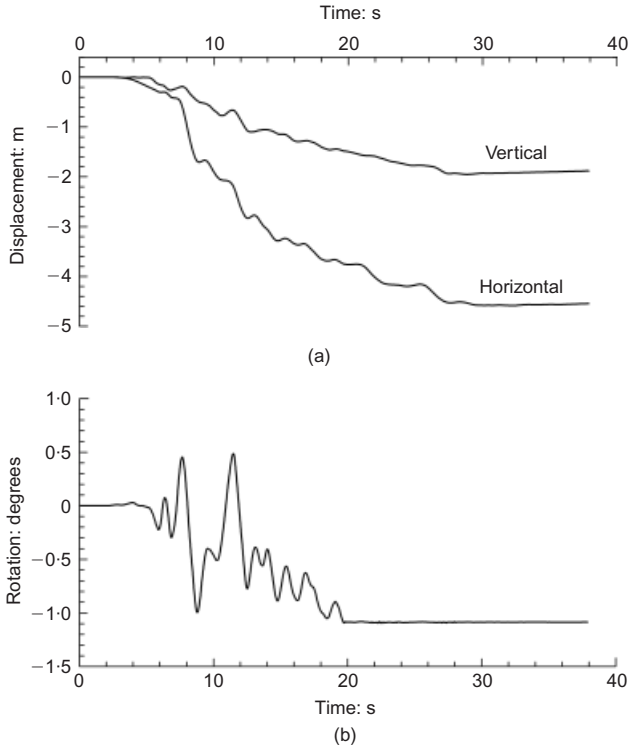

Fig. 6. (a) Computed horizontal and vertical displacement time histories at upper sea-side corner of caisson; (b) computed rotation time history of caisson (backfill and foundation rubble: $k = 4 \times 10^{-4}$ m/s, $D_r = 40\%$)

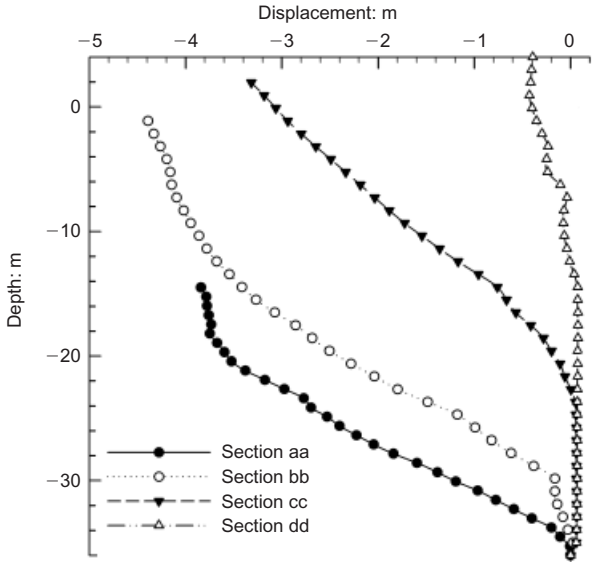

Fig. 7. Distribution of horizontal displacements along sections aa, bb, cc and dd at end of shaking (position of each section is shown in Fig. 3)

pore water pressure and of plastic shear strain (Figs 8 and 9). Notice that the deformation of the foundation soil underneath the caisson caused most of the horizontal movement of the wall; no slippage was computed to have occurred between the caisson and the foundation rubble, in agreement with the findings in small-scale shaking-table tests by Ghalandarzadeh *et al.* (1998). The deformation pattern of the foundation rubble indicates a reduced bearing capacity of the foundation soil under significant moment and lateral loading from the heavy and tall wall. Such a reduction in bearing capacity appears to be an important deformational mechanism that contributed significantly to the large rotation of the wall. Indeed, observe in Fig. 9 that already at $t \approx 7{\cdot}5$ s, just in the middle of the first significant acceleration pulse (with $A \approx 0{\cdot}20g$ and $\Delta t \approx 2$ s in the ground surface record of Port Island; Fig. 4), plastic strains in the foundation soil in front of the wall reach a substantial 5%, which indicates plastification of the material. The maximum plastic strain reaches 30% at the end of shaking, and is concentrated in the upper layer of the foundation soil, near the seaward wall toe. Notice that the entire mass of the foundation soil to the left of the wall is compressed horizontally and extended vertically, whereas the foundation soil beneath the wall material is compressed vertically (as the wall sinks) and extended horizontally. Thus the deformation mode in the foundation soil is a combination of plane strain extension and shearing.

Several other observations can be made in Fig. 7. First, the permanent outward displacements at section dd (free field), and even at section cc (a mere 22 m from the back of the wall), are primarily displacements in the backfill rather than in the underlain clay layer. In section cc only about 0·65 m out of 3·30 m total surface displacement occur in the clay. As we approach the caisson, however (section bb), this trend reverses: about 3·40 m out of the 4·45 m total top displacement already takes place in the foundation soil—an indication of the crucial role of deformation and yielding of the underlying foundation soil.

Second, we notice that the computed permanent outward displacement at the surface extends all the way to the end of our model, at about 100 m from the wall (displacement $\approx$ 0·40 m). This is consistent with the observation of the extent of 'lateral spreading' over distances of 100–200 m from the back of quay walls (Ishihara, 1997).

Figure 8 plots the contours of excess pore water pressure ratio, which is redefined, compared with equation (11), as

$$r_u^* = \frac{\Delta u}{\sigma'_{0m}} \tag{12}$$

where Δu is the excess pore water pressure and σ'_{0m} is the initial mean effective stress. The distribution of r_u^*, given at times $t = 7{\cdot}5$, 9, 30 and 38 s, shows that high pore water pressure ratios develop both in the free field *and* beneath the caisson. Moreover, the left part of the foundation soil is compressed and sheared as the left side of the wall settles deeper into the foundation soil, leading to excess pore water pressure ratios that exceed the value of 0·80. Fig. 10 plots the time histories of the ratio r_u^* at the four points A, B, C and D shown in Fig. 3. The following observations are noteworthy.

(*a*) The highest excess pore water pressure ratio, very close to 1, develops in the free field point D. Notice the relatively slow rate of pressure accumulation.

(*b*) By contrast, in the backfill point C, located at the same depth as D but only 22 m from the back of the wall, the excess pore water pressure ratio r_u^* attains large negative values ($\approx -0{\cdot}60$) and strongly oscillatory behaviour during the period of intense shaking. After $t \approx 12$ s r_u^* starts increasing, and gradually accumulates to a level of about +0·40. This behaviour is due to the stress reduction that develops in this region as the wall moves outward (seaward) in an 'active' fashion. The associated tendency of the soil to dilate is translated into negative pore water pressures under constant-volume (undrained) conditions. Notice the big negative increments in pore water pressure in the time internal of 6–12 s, just when the long-duration acceleration pulses in the excitation (Fig. 4) cause the largest outward movement of the wall (Fig. 6). Qualitative

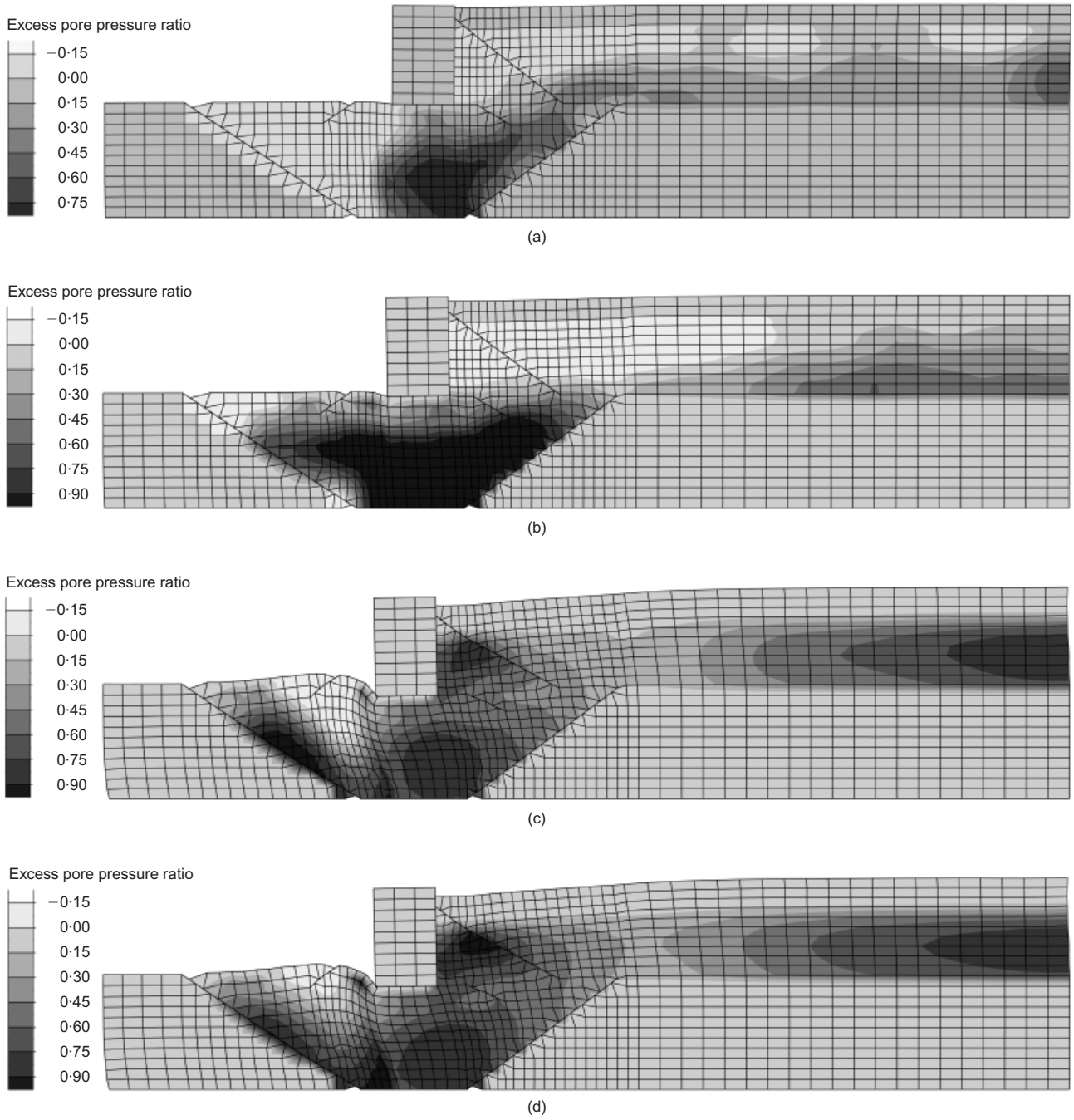

Fig. 8. Contours of excess pore water pressure ratio at various times t: (a) 7·5 s; (b) 9 s; (c) 30 s; (d) 38 s (backfill and foundation rubble: $k = 4 \times 10^{-4}$ m/s, $D_r = 40\%$)

experimental support for such strongly negative pore water pressures is discussed later in the paper.

(*c*) Point B exhibits a pore water pressure response of a somewhat intermediate nature, between the responses of C and D. From 6 to 8 s r_u^* reaches a plateau of about 0·70 (see explanation below). Later on, when there is a significant seaward movement of the wall, a large temporary reduction in r_u takes place, after which the ratio gradually builds up and approaches the residual value of 0·70.

(*d*) Point A, located on the caisson centreline at about 12 m underneath its base, develops an r_u^* ratio of about 0·80 very quickly after $t \approx 6$ s (compared with the slower build-up in the free-field point D). This is apparently the result of the additional shear stresses developing owing to the large inertia force experienced by the wall and the backfill upon the arrival of the first long-duration acceleration pulses at t $\approx$ 6–7 s. Eventually, the ratio slowly approaches the value of 0·90.

(*e*) In the 10 s after the end of shaking (i.e. $t = 30$–40 s) there occurs a redistribution of pore water pressures, as water flows *towards* point C (which at $t = 30$ s had a relatively small water pressure) and *away* from point A (which had a relatively large water pressure) compared with other points in their immediate neighbourhood.

The overall response is consistent with the observed behaviour in Rokko and Port Islands. Specifically, it was indeed observed that

(*a*) no liquefaction occurred near the quay wall that failed.

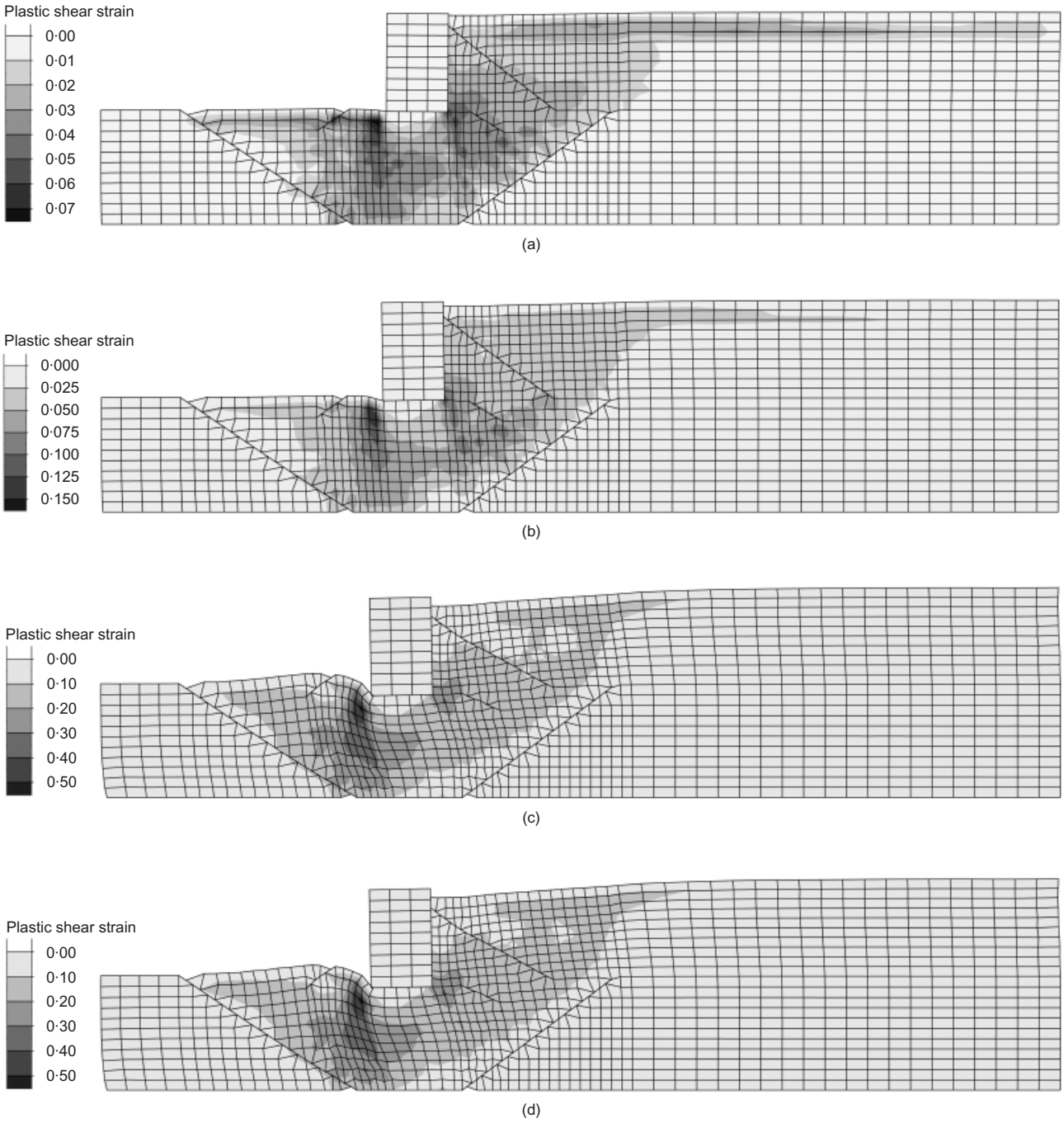

Fig. 9. Contours of accumulated plastic shear strain at various times *t*: (a) 7·5 s; (b) 9 s; (c) 30 s; (d) 38 s (backfill and foundation rubble: $k = 4 \times 10^{-4}$ m/s, $D_r = 40\%$)

(*b*) liquefaction occurred in the (unimproved) fill material in the free field
(*c*) all the walls moved and rotated outwards (seawards)
(*d*) the soil surface in front of the toe of the wall heaved substantially (e.g. Ishihara *et al.*, 1996; Towhata *et al.*, 1996).

Moreover, the numerical values computed with the modified Pastor model in conjunction with the finite-difference algorithm are in general agreement with earlier results presented by Iai *et al.* (1998) based on a different constitutive model and a finite element formulation. Note that the latter analysis used 20 s of earthquake shaking and computed that the upper left corner of the wall had moved 3·5 m seawards. In the present analysis the movement at that same time is about 3·8 m. Pore water pressure ratios in the free field and the foundation soil are about 0·90 and 0·80 respectively in the *two* analyses. The only poor agreement is in the rotation of the wall: 1° (in our analysis) compared with 4° (Iai *et al.*, 1998) and 5° (measured). An attempt to shed light on the possible causes of this discrepancy is described later on in this paper.

A case with instrumental evidence of the possibility of *strongly negative* pore water pressures developing behind a quay wall has been published (Lee, 2005). For a quay wall similar to the studied one in the harbour of Taichung, Taiwan, which experienced a 1·7 m outward displacement during the Chi-Chi 1999 M_w 7·7 earthquake, Lee conducted a series of parametric centrifuge tests (at 120*g* level) in the facility of Rensselaer Polytechnic Institute (in Troy, New York). He repeatedly recorded negative pore water pressures behind the wall, depending on the backfill permeability. For the case of a 'small enough' coefficient of permeability of the backfill soil, these negative pore water pressures were

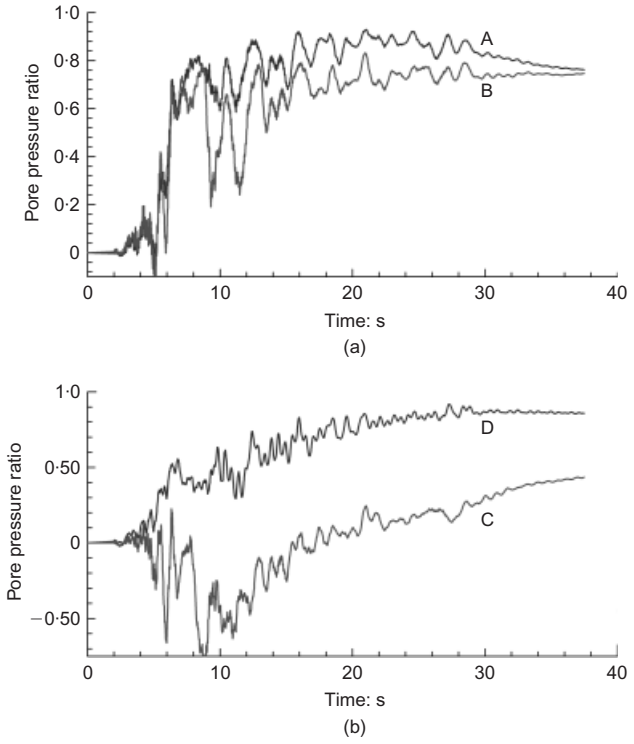

Fig. 10. Evolution of pore water pressure ratio during shaking (backfill and foundation rubble: $k = 4 \times 10^{-4}$ m/s, $D_r = 40\%$): (a) points A and B; (b) points C and D

substantial: their permanent (inelastic) component reached values corresponding to an $r_u \approx -0{\cdot}60$, while their instantaneous total values amounted up to $r_u^* = -1$. In interpreting these measurements he noted that the soil elements behind the wall develop alternately positive and negative values of Δu. The negative values are more significant because lateral extension (LE) dominates as the wall gradually moves outward. He concluded that the LE undrained stress path 'arrests' the pore water pressure build-up and results in r_u^* values as low as -1. This independent experimental finding of 'suction' behind the wall provides an important corroboration (qualitative at least) of our numerical study.

Earth and water pressures versus Mononobe–Okabe

Figures 11 and 12 plot respectively the distributions (at $t = 7{\cdot}5$, 9, 13, 30 and 38 s) of the effective static-plus-dynamic earth pressure and of the pore water pressure against the back of the quay wall. In addition, we plot for comparison the conventional Mononobe–Okabe (M-O) static-plus-dynamic curve for $\Delta u = 0$, as well as the approximate Coulomb static effective earth pressure distribution, under the aforesaid 'homogenisation' approximation described through equation (6). The dynamic components of the effective earth pressure (equation (10)) were plotted assuming they are distributed uniformly along the height.

To our surprise, the conventional pseudo-static M-O approximation to this complicated problem leads to active earth pressures that are in good agreement with the numerically computed distributions during the strongest part of excitation ($t = 7{\cdot}5$–13 s). In fact, notice that in the early stages of shaking ($t \approx 7{\cdot}5$ s), when the wall had moved outwards but had experienced very small rotation (Fig. 6), the numerical dynamic pressures were strongly concentrated on the upper half of the wall; the resultant dynamic force was located at about $0{\cdot}60H$ from the base, in accord with both the Veletsos & Younan (1997) analysis for rigid non-rotating walls (see also Wood, 1975; Gazetas *et al.*, 2004)

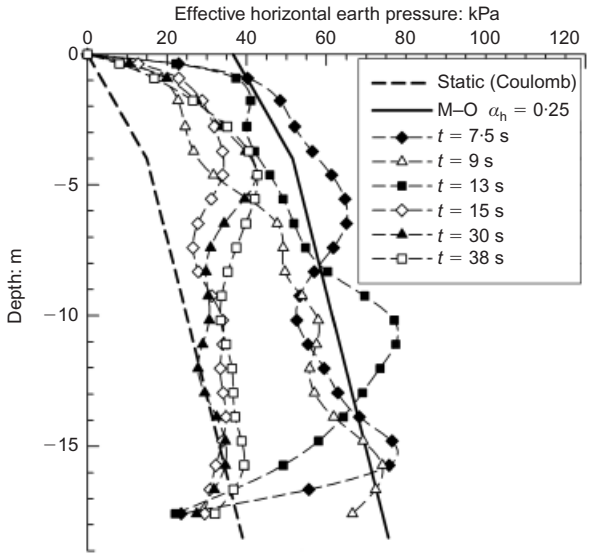

Fig. 11. Effective static plus dynamic earth pressure behind wall at times $t = 7{\cdot}5$ s, 9 s, 13 s, 15 s, 30 s and 38 s; comparison of numerical predictions with Coulomb (static) and Mononobe–Okabe (static plus dynamic) pressures

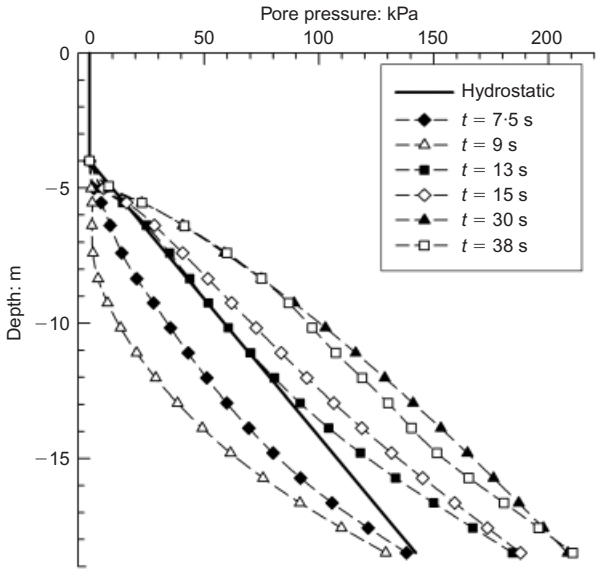

Fig. 12. Net pore water pressures (static plus dynamic) behind wall at times $t = 7{\cdot}5$ s, 9 s, 13 s, 15 s, 30 s and 38 s

and the small-scale experiments cited by Seed & Whitman (1970) as a justification for their recommendations.

At $t = 9$ s, when the seaward rotation just passed through its local maximum value of about 1°, the dynamic earth pressures were invariably (but only slightly) smaller than those of M-O, and were distributed almost uniformly, with their resultant at $\frac{1}{2}H$ from the base—again in accord with the Veletsos & Younan (1997) solution for a rigid wall rotating about its base.

At later times the earth pressures change in response to changes in wall motion and pore water pressure. The distribution of the latter along the height is not far from triangular. At $t = 9$ s, when nearly the largest outward rotation takes place, at small depths (from -4 to -9 m), $\Delta u \approx -\gamma_w z$, and thereby the net water pressure $u_0 + \Delta u$, vanishes.

Much later, at $t > 13$ s, a 'contamination' of the region behind the wall with 'migrating' positive pore water pressures takes place, arising mainly from the water inflow from the (nearly or fully) liquefied nearby regions. The total water pressures eventually exceed the hydrostatic values by as

much as 30%, but liquefaction is not even imminent; effective earth pressures in Fig. 11 remain slightly higher than the initial (static) active earth pressures, having achieved an almost uniform distribution with depth.

Finally, the evolution with time of the resultant static-plus-dynamic force resolved into its two components, effective and water force, is portrayed in Fig. 13. Observe that the Coulomb plus Mononobe–Okabe pseudo-static total force is a good approximation of the largest exerted effective force on the wall.

POSSIBLE CAUSES OF OUR UNDERPREDICTION OF THE ACTUAL OUTWARD ROTATION

One question remains unanswered: why, despite such a good performance of the numerical analysis, is the angle of permanent outward rotation (tilt) of the quay wall so poorly 'predicted' (1° compared with 4° or 5°)?

One must first realise that if it is not an easy task to determine the rotation of simple retaining walls (Whitman, 1990; Steedman & Zeng, 1996; Al-Homoud & Whitman, 1999), reliably computing the residual rotation of a quay wall of the type examined here in the realm of large soil deformation and liquefaction would be a formidable undertaking. As an example, we refer to the experimental study by Ghalandarzadeh *et al.* (1998), who have demonstrated with small-scale tests that it is difficult, not only *quantitatively* but even *qualitatively*, to predict wall rotation. They discovered the following.

(*a*) A caisson may tilt *forwards* (i.e. seawards, as in the studied case) or *backwards* depending on several factors, the most profound of which are the weight of the caisson, the intensity of shaking, and the stiffness/strength of the foundation and backfill soil.

(*b*) *Light* caissons tilt backwards, moving together with the backfill and foundation soil—a situation reminiscent of the classical wedge rotation on a circular slip surface passing through the retained and the foundation soil. In Kobe only 2 (out of about 200) quay walls experienced this mode of 'failure'.

(*c*) *Heavy* caissons tilt forwards, mainly because large overturning moments develop and impose contact pressures at their toe that are very high, leading to local shear failure and 'penetration' of the toe into the soil. In Kobe almost all quay walls experienced this mode of 'failure'.

(*d*) Exceptions to the above rules abound, as several other parameters influence the response. For instance, light caissons under weak shaking would usually experience forward rather than backward tilting; if the foundation soil is very stiff, permanent tilting would be negligible, and only horizontal 'sliding' displacements might be significant.

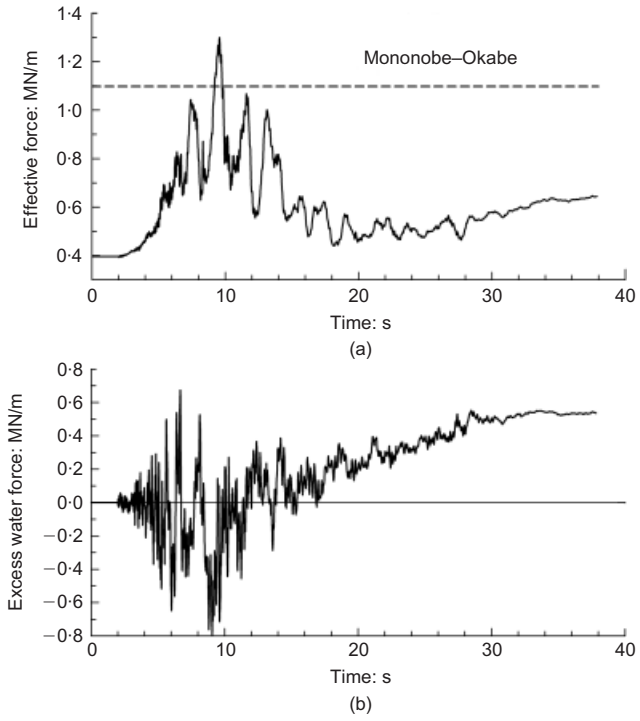

Fig. 13. Evolution of (a) effective static-plus-dynamic force, (b) excess water force acting on back of wall during shaking

In light of all this, and after carefully studying the various sources of uncertainty in our analyses, we concluded that the following two factors might (among others) have been responsible for our underprediction: (a) the stiffness (and relative density) of the soil under the toe of the caisson could have been locally smaller (e.g. as a result of the prevailing static shear stresses); (b) the stiffness of the backfill soil active wedge might have been (slightly) higher.

This latter cause may seem paradoxical: increasing the stiffness (e.g. by increasing the relative density) of the retained soil should have been a way of *improving* the performance of the system, not *worsening* it. This paradox may be resolved as follows. As is well understood, the denser material in the active soil wedge is also (more) *dilatant* (e.g. Bolton, 1986): hence upon shearing under undrained conditions it will tend to develop more negative pore water pressures. These pressures will be added to the negative effective pressures caused by the lateral stress reduction (active conditions), as was the case with the loose ($D_r = 40\%$) soil studied so far. Indeed, this behaviour is illustrated in Figs 14, 15 and 16, which should be compared with Figs 5, 6 and 12 respectively. They refer to the same quay wall and soil as in the preceding study, except that the relative density of the rubble in the backfill and the foundation is increased to $D_r = 60\%$. We would not argue that this indeed was the physical reality in Kobe; only that this value represents one plausible scenario. The following conclusions can be drawn from these figures.

(*a*) The rotation of the caisson is now much larger, exceeding 4°, although the outward horizontal displacement of the wall (even of its top, suffering the most from this rotation) has decreased.

(*b*) Negative pore water pressures are computed to be about equal to or even to exceed in absolute value the hydrostatic water pressures. The net water pressure may thus be (slightly) negative at depths of 8–17 m. This inward 'suction' acting on the lower part of the wall produces a counterclockwise increment of overturning moment on the wall—which may explain this possible negative role of the increasing backfill stiffness in our analysis.

We shall not argue that the above findings constitute a definitive proof of this 'peculiar' role of soil density. This remains only as a reasonable hypothesis that should await considerably more testing (analytical, experimental and observational) before being verified, modified, or even refuted. We merely note that the characterisation as 'paradox' applies *only* to rotation; in contrast, the increase in density of the rubble to 60% did in fact *reduce* the overall displacement of the wall, as well as the settlement of the backfill. Understandably, increasing the density of *all* the retained (backfilled) soil to $D_r = 75\%$ would have prevented liquefaction from occurring, and would have led to a (maximum $\approx$

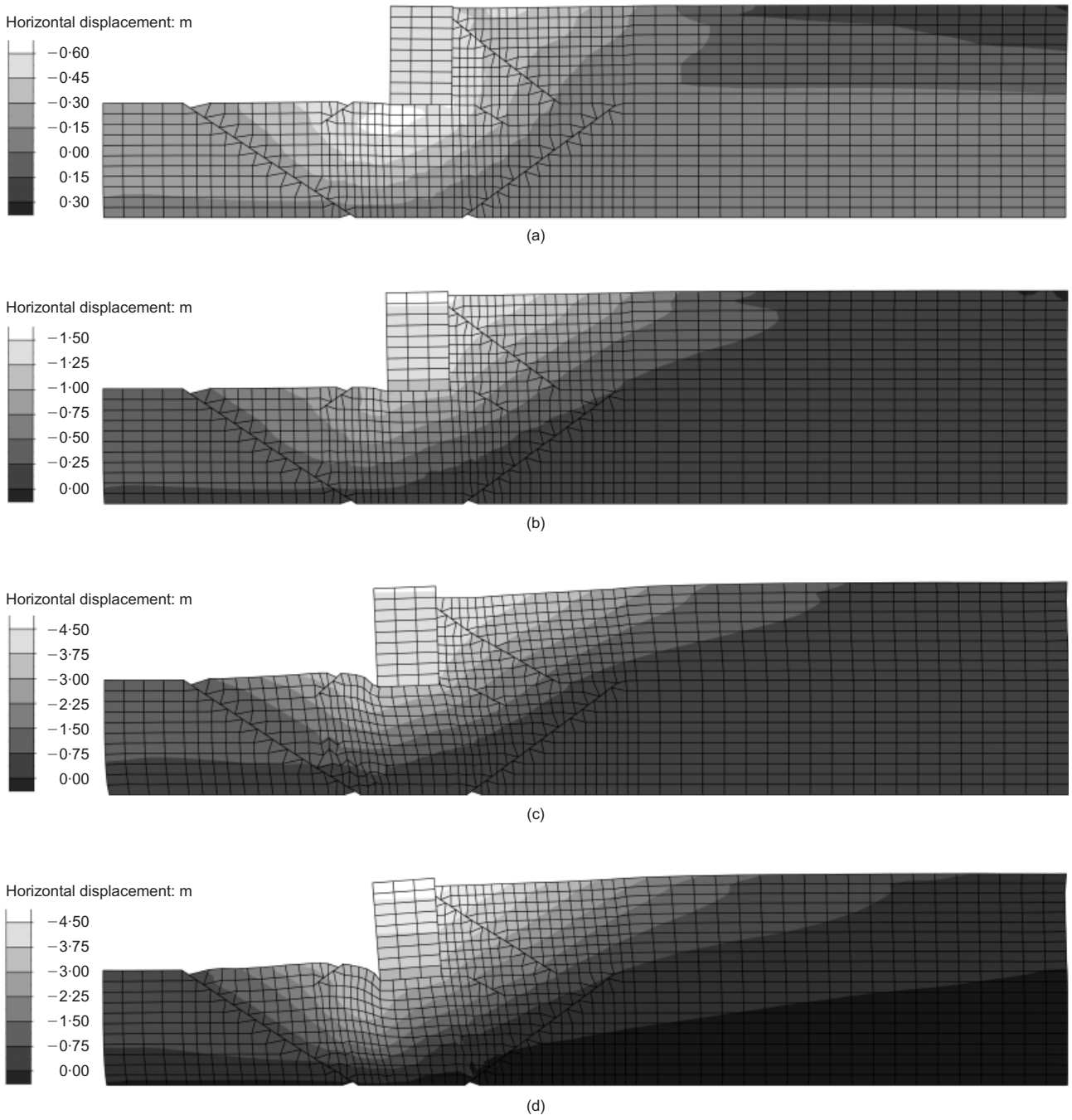

Fig. 14. Deformed geometry and contours of horizontal displacements of the quay wall at various times t: (a) 7·5 s; (b) 9 s; (c) 30 s; (d) 38 s (backfill and foundation rubble: $k = 4 \times 10^{-4}$ m/s, $D_r = 60\%$)

residual) displacement of the wall of only 2·5 m (Dakoulas & Gazetas, 2005a, 2005b).

CONCLUSIONS

The following conclusions may be drawn from this study.

(*a*) The seismic behaviour of caisson-type quay walls is a complex phenomenon, as it depends on the interplay of the following simultaneously acting factors
  (i) the oscillatory wall inertia force and earth pressures, causing outward displacement and rotation of the wall due to the compliance of the supporting (foundation) soil
  (ii) the generation of positive excess pore water pressures in the loose (underwater-placed) soils, both in the free field and in the foundation
  (iii) the deformation, yielding and 'squeezing out' of the foundation soil
  (iv) the extensional deformation of the backfill soil adjacent to the wall, as the wall moves outward, causing negative excess pore water pressures ('suction') that may even exceed in absolute terms the positive hydrostatic values
  (v) the continuous dissipation and redistribution of pore water pressures in the retained and foundation soil.

(*b*) An effective stress analysis of the behaviour of an idealised Rokko Island quay wall in Kobe (Japan) during the 1995 earthquake, based on a numerical code and a comprehensive constitutive soil model, has shown very good quantitative agreement with field observations (reported by several Japanese researchers) of

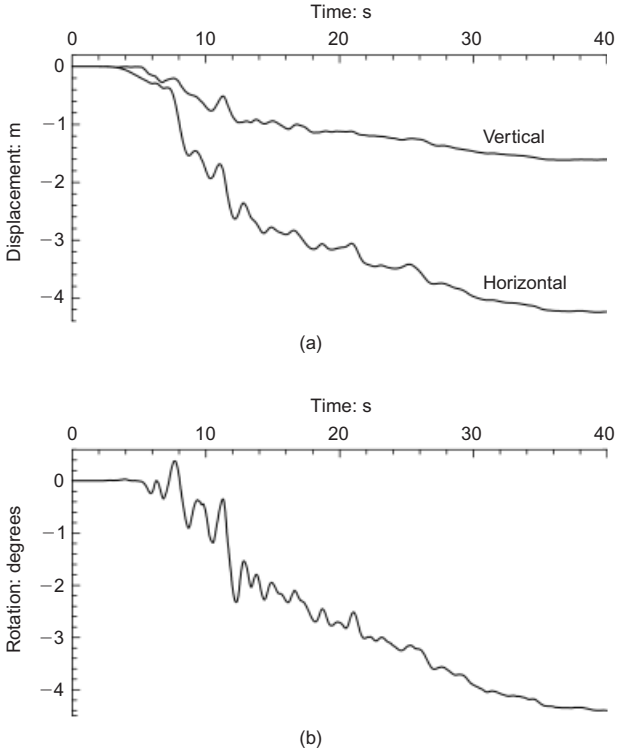

Fig. 15. (a) Computed horizontal and vertical displacement time histories at upper sea-side corner of caisson; (b) computed rotation time history of caisson (backfill and foundation rubble: $k = 4 \times 10^{-4}$ m/s, $D_r = 60\%$)

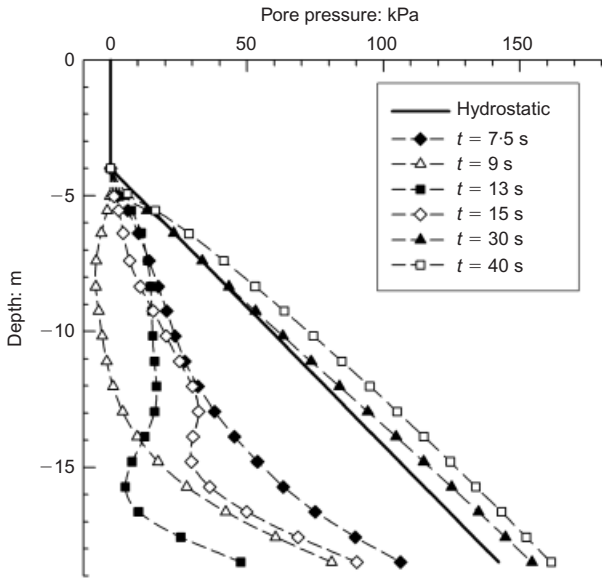

Fig. 16. Net pore water pressures (static plus dynamic) behind wall at times $t = 7{\cdot}5$ s, 9 s, 13 s, 15 s, 30 s and 40 s (backfill and foundation rubble: $k = 4 \times 10^{-4}$ m/s, $D_r = 60\%$)

(i) the seaward horizontal displacement of the wall
(ii) the settlement of the wall and the backfill soil
(iii) the non-occurrence of liquefaction in a backfill zone behind the wall
(iv) the substantial heave of the soil surface at the sea bottom, in front of the toe of the wall.

Moreover, the analysis predicts successfully the permanent horizontal displacements and the occurrence of liquefaction in the far field (about 100 m behind the wall). However, the wall rotation was substantially underpredicted in our initial analyses.

(*c*) During the strongest part of excitation, as the wall moves seawards, *negative* excess pore water pressures develop behind the wall, as a result of substantial lateral extension imposed on the soil. These excess (dynamic) pressure increments may (locally and instantaneously) result in zero, or even negative, *net* pore water pressures.

(*d*) The rotation of the wall (both its direction [outward or inward] and magnitude) seems to be a sensitive function of a number of factors, including
(i) the stiffness/density of both the underlying and the retained soil
(ii) the coefficients of permeability of the soils
(iii) the weight of the caisson and its distribution along the height
(iv) the intensity and frequency content of ground shaking.

Whereas the effect of most of the above factors has been demonstrated by several researchers in the literature, we have only explored here the role of the relative density of the backfill rubble. It was shown that, as the latter increased, higher negative pressures developed and thus 'suction' of the lower part of the wall increased wall rotation, which almost reached the observed levels (of about 4–5°). However, it is felt that considerable additional testing (analytical, experimental and observational) is needed before adopting such a conclusion.

(*e*) Active earth pressures computed with the conventional pseudo-static Mononobe–Okabe method (for a seismic coefficient equal to 0·25, corresponding to the effective peak ground acceleration) are, surprisingly and somewhat fortuitously, in accord with the numerically computed earth pressure distributions during the strongest part of excitation.

(*f*) The resultant of the dynamic force is located at a height of about $0{\cdot}60H$ from the base for small wall rotations and at about $0{\cdot}50H$ for larger wall rotations, in accordance with earlier published small-scale shaking experiments for dry soil. This agreement is rather surprising: in view of the outward rotation of the wall, a more triangular distribution of earth pressures prevails, consistent with a lower point of application of the resultant (Veletsos & Younan, 1997). However, this may be merely a coincidence; a plausible cause: the aforementioned large 'suction' at the lower half of the wall increases the overturning moment while reducing the resultant horizontal force, thereby increasing the height of application of the resultant.

A few centrifuge and small-scale shaking experiments in the published literature offer a strong qualitative corroboration to the above conclusions.

NOTATION

A	peak ground acceleration
D_r	relative density
e	void ratio
$G_{\max}$	shear modulus at small strains
g	acceleration of gravity
H	height of wall
H_{sur}	height of wall above water table
H_w	height of wall below water table
H_U	modulus for unloading
H_U^*	modified modulus for unloading
H_{u0}	constitutive model parameter*
H_0	constitutive model parameter*
$J_2^{\varepsilon p}$	second invariant of the deviatoric plastic strain

K_A	active earth pressure coefficient
K_{AE}	dynamic active earth pressure coefficient
K_0	constitutive model parameter*
k	permeability
M_{fc}	constitutive model parameter*
M_{gc}	constitutive model parameter*
M_s	earthquake magnitude
P_h	hydrodynamic force
p'	mean effective stress
p_a	atmospheric pressure
q	deviator stress
$r_u = \Delta u/\sigma'_{v0}$	excess pore water pressure ratio based on effective vertical stress σ'_{v0}
$r_u^* = \Delta u/\sigma'_{0m}$	excess pore water pressure ratio based on mean effective stress σ'_{0m}
W	weight of wall
α	constitutive model parameter*
$\alpha_h,\ \alpha_v$	seismic coefficient in the horizontal and vertical direction
α'_h	apparent seismic coefficient
β_0	constitutive model parameter*
β_1	constitutive model parameter*
γ	constitutive model parameter*
γ	unit weight of soil
$\gamma',\ \gamma_e$	effective unit weight
γ_b	buoyant unit weight of soil
γ_u	constitutive model parameter*
γ_{sat}	saturated unit weight of soil
γ_{we}	effective unit weight of water
Δu	excess pore water pressure
δ	friction angle at wall – rubble interface
ε_s^p	plastic shear strain
$\eta = q/p'$	stress ratio
η_u	stress ratio at unloading
$\sigma'_0,\ \sigma'_{0m},$	initial mean effective stress
$\sigma'_{v0},$	initial vertical effective stress
ϕ	friction angle

* The definitions of the model parameters and the associated equations are given in original paper by Pastor *et al*. (1990)

REFERENCES

Al-Homoud, A. S. & Whitman, R. V. (1999). Seismic analysis and design of rigid bridge abutments considering rotation and sliding incorporating nonlinear soil behaviour. *Soil Dynam. Earthquake Engng* **18**, No. 4, 247–277.

Bolton, M. D. (1986). The strength and dilatancy of sands. *Géotechnique* **36**, No. 1, 65–78.

Cubrinovski, M. & Ishihara, K. (1999). Empirical correlation between SPT *N*-value and relative density for sandy soils. *Soils Found.* **39**, No. 5, 61–71.

Dakoulas, P. (2003). *Verification of a constitutive model for noncohesive soils*, Research Report. Volos, Greece: University of Thessaly (in Greek).

Dakoulas, P. & Gazetas, G. (2005a). Effective stress analysis of caisson quay walls: application to Kobe. *Soils Found.* **45**, No. 4, 133–147.

Dakoulas, P. & Gazetas, G. (2005b). Dynamic earth and water pressures in the foundation and the backfill of quaywalls. *Proc. 1st Greece–Japan Workshop on Seismic Design, Observation and Retrofit of Foundations, Athens*, 165–183.

Ebeling, R. M. & Morison, E. E. (1992). *The seismic design of waterfront retaining structures*, Technical Report ITL-92-11. Washington, DC: US Army Corps of Engineers.

Fujiwara, T., Horikoshi, K. & Sueoka, T. (1999). Centrifuge modeling of dynamic earth pressure acting on gravity type wall during large earthquake. *Proc. 2nd Int. Conf. on Earthquake Geotechnical Engineering*, Lisbon **1**, 401–406.

Gazetas, G., Dakoulas, P. & Dennehy, K. (1990). Empirical seismic design method for waterfront anchored sheetpile walls. In *Design and performance of earth retaining structures*, pp. 232–250. Ithaca: American Society of Civil Engineers.

Gazetas, G., Psarropoulos, P., Anastasopoulos, I. & Gerolymos, N. (2004). Seismic behaviour of flexible retaining systems subjected to short-duration moderately strong excitation. *Soil Dynam. Earthquake Engng* **24**, No. 7, 537–550.

Gazetas, G., Anastasopoulos, I. & Dakoulas, P. (2005). Failure of harbour quaywalls in the Lefkada 2003 earthquake. In *Performance based design in earthquake geotechnical engineering: Concepts and Research, Proceedings of the Geotechnical Earthquake Engineering Satellite Conference*, pp. 62–69. Osaka: Japanese Geotechnical Society.

Ghalandarzadeh, A., Orita, T., Towahata, I. & Yun, F. (1998). Shaking table tests on seismic deformation of gravity quaywalls. *Soils Found.* (Special issue on geotechnical aspects of the January 17, 1995 Hyogoken-Nambu earthquake), **2**, 115–132.

Hamada, M. & Wakamatsu, K. (1996). Liquefaction, ground deformation and their caused damage to structures. In *The 1995 Hyogoken-Nanbu Earthquake*, pp. 45–91. Tokyo: Committee of Earthquake Engineering, Japan Society of Civil Engineers.

Iai, S. (1998). Seismic analysis and performance of retaining structures. In *Geotechnical earthquake engineering and soil dynamics III* (eds P. Dakoulas, M. K. Yegian and R. Holtz), Geotechnical Special Publication, Vol. II, pp. 1020–1044. American Society of Civil Engineers.

Iai, S., Ichii, K., Liu, H. & Morita, T. (1998). Effective stress analysis of port structures. *Soils Found.* (Special issue on geotechnical aspects of the January 17, 1995 Hyogoken-Nambu earthquake), **2**, 97–114.

Inagaki, H., Iai, S., Sugano, T., Yamazaki, H. & Inatomi, T. (1996). Performance of caisson type quay walls at Kobe port. *Soils Found.* (Special issue on geotechnical aspects of the January 17, 1995 Hyogoken-Nambu earthquake), **1**, 119–136.

Ishihara, K. (1997). Terzaghi oration: Geotechnical aspects of the 1995 Kobe earthquake. *Proc. 14th Conf. Soil Mech. Found. Engng, Hamburg* **4**, 2047–2073.

Ishihara, K., Yasuda, S. & Nagase, H. (1996). Soil characteristics and ground damage. *Soils Found.* (Special issue on geotechnical aspects of the January 17, 1995 Hyogoken-Nambu earthquake), **1**, 109–118.

Itasca (2000). *Fast Lagrangian Analysis of Continua, User's Manuals*. Minneapolis: Itasca Consulting Group.

Iwasaki, Y. & Tai, M. (1996). Strong motion records at Kobe Port Island. *Soils Found.* (Special issue on geotechnical aspects of the January 17, 1995 Hyogoken-Nambu earthquake), **1**, 29–40.

JSCE (2000). *Earthquake resistant design codes in Japan*. Tokyo: Japan Society of Civil Engineers.

Kamon, M., Wako, T., Isemura, K., Sawa, K., Mimura, M., Tateyama, K. & Kobayashi, S. (1996). Geotechnical disasters on the waterfront. *Soils Found.* (Special issue on geotechnical aspects of the January 17, 1995 Hyogoken-Nambu earthquake), **1**, 137–147.

Kitajima, S. & Uwabe, T. (1978). Analysis on seismic damage in anchored sheet-piling bulkheads. *Report of the Port and Harbor Research Institute* **18**, No. 1, 67–130 (in Japanese).

Lee, C. J. (2005). Centrifuge modeling of the behavior of caisson-type quay walls during earthquakes. *Soil Dynam. Earthquake Engng* **25**, No. 2, 117–131.

Matsuzawa, H., Ishibashi, I. & Kawamura, M. (1985). Dynamic soil and water pressures of submerged soils. *J. Geotech. Engng ASCE* **111**, No. 10, 1161–1176.

Mononobe, N. & Matsuo, H. (1929). On the determination of earth pressures during earthquakes. *Proceedings of the World Engineering Congress, Tokyo*, pp. 177–185.

Noda, S., Uwabe, T. & Chiba, T. (1975). Relation between seismic coefficient and ground acceleration for gravity wall. *Report of the Port and Harbor Research Institute, Japan* **14**, No. 4, 67–111 (in Japanese).

OCDI (2002). *Technical standards and commentaries for port and harbor facilities in Japan.* Tokyo: The Overseas Coastal Area Development Institute of Japan.

Okabe, S. (1926). General theory of earth pressures. *J. Jpn. Soc. Civ. Engng* **12**, No. 1.

Pastor, M. & Zienkiewicz, O. C. (1986). A generalized plasticity hierarchical model for sand under monotonic and cyclic loading. In *Numerical methods in geomechanics* (eds G. N. Pande and W. F. Impe), pp. 131–150. London: John Wiley.

Pastor, M., Zienkiewicz, O. C. & Chan, A. C. H. (1990). Generalized plasticity and the modelling of soil behaviour. *Int. J. Numer. Anal. Methods Geomech.* **14**, No. 3, 151–190.

Pastor, M., Zienkiewicz, O. C. & Leung, K. H. (1985). Simple model for transient soil loading in earthquake analysis II: Non-associative models for sands. *Int. J. Numer. Anal. Methods Geomech.* **9**, No. 5, 477–498.

PIANC (2001). *Seismic design guidelines for port structures*. Tokyo: A. A. Balkema Publishers.

Sato, M., Watanabe, H. & Katayama, S. (1998). Study on mechanism of caisson type sea wall movement during earthquakes. *Proc. 4th Conf. on Case Histories in Geotechnical Engineering, St Louis*, **1**, 604–611.

Seed, R. B. & Whitman, R. (1970). Design of earth retaining structures for dynamic loads. *Proceedings of the specialty conference on lateral stresses in the ground and design of earth retaining structures*, pp. 103–147. Ithaka: American Society of Civil Engineers.

Somerville, P. (1998). Emerging art: earthquake ground motion. In *Geotechnical earthquake engineering and soil dynamics III* (eds P. Dakoulas, M. K. Yegian and R. Holtz), Geotechnical Special Publication, Vol. 1, pp. 1–38. Seattle: American Society of Civil Engineers.

Steedman, R. S. & Zeng, X. (1996). Rotation of large gravity walls on rigid foundations under seismic loading. In *Analysis and design of retaining structures against earthquakes* (ed. S. Prakash, Geotechnical Special Publication No. 60, pp. 38–56. ASCE.

Sugano, T., Mitoh, M. & Oikawa, K. (1995). *Mechanism of damage to port facilities during the 1995 Hyogo-ken Nanbu earthquake: Experimental study on the behavior of caisson-type quay wall during earthquake using underwater shaking table*, Technical Note of the Port and Harbor Research Institute, No. 813. Tokyo: Ministry of Transport.

Torii, T. & Tatsuoka, F. (1982). A study of triaxial liquefaction strength of gravelly soil. *Proceedings of Annual Meeting, Japanese Society for Soil Mechanics and Foundation Engineering*, 1669–1672.

Towhata, I., Ghalandarzadeh, A., Sundarraj, K. & Vargas-Monge, W. (1996). Dynamic failures of subsoils observed in waterfront areas. *Soils Found.* (Special issue on geotechnical aspects of the January 17, 1995 Hyogoken-Nambu earthquake), 149–160.

Veletsos, A. S. & Younan, A. H. (1997). Dynamic response of cantilever retaining walls. *J. Geotech. Geoenviron. Engng ASCE* **123**, 161–172.

Westergaard, H. M. (1933). Water pressures on dams during earthquakes. *Trans. ASCE* **98**, 418–433.

Whitman, R. (1990). Seismic design behaviour of gravity retaining walls. *Proceedings of the ASCE conference on design and performance of earth retaining structures*, Geotechnical Special Publication No. 25, pp. 817–842.

Wood, J. H. (1975). Earthquake-induced pressures on a rigid wall structure. *Bull. N. Z. Nat. Earthquake Engng* **8**, No. 3, 175–186.

Zeng, X. (1993). Experimental results of Model No. 11. *Proceedings of the symposium on verification of numerical procedures for the analysis of soil liquefaction problems*, University of California Davis, Vol. 1, pp. 895–908.

Zienkiewicz, O., Leung, K. H. & Pastor, M. (1985). Simple model for transient soil loading in earthquake analysis I: Basic model and its application. *Int. J. Numer. Anal. Methods Geomech.* **9**, No. 5, 453–476.

Zienkiewicz, O. C., Chan, A. H. C., Pastor, M., Schrefler, B. A. & Shiomi, T. (1999). *Computational geomechanics with special reference to earthquake engineering*. New York: John Wiley.

Zienkiewicz, O. C., Pastor, M., Chan, A. H. C. & Xie, Y. (1991). *Computational approaches to the dynamics and statics of saturated and unsaturated soils*, Advances in Geotechnical Analysis, Development in Soil Mechanics and Foundation Engineering, **4** (eds P. Banerjee and R. Butterfield), pp. 151–190. Oxford: Elsevier.